hexagon:2611.01276v1

PEDRO'S DICE: A QUANTUM APPROACH. QUANTUM DATA STATISTICS ON GRAPHS, SPECTRAL READINESS, AND THE EXACTLY SOLVABLE 26-STATE CUBE

PEDRO CACERES

Abstract. A die is usually reduced to six equiprobable outcomes, but a physical cube has 26 resting configurations (6 faces, 12 edges, 8 vertices) joined by a graph, and the question that matters is how ready it is to change what it shows. We answer it with Quantum Data Statistics (QDS) on a graph of states, keeping the canonical objects of QDS: the amplitude $\psi = \sqrt{p}$, a Hamiltonian with ground state $H\psi = 0$, the propagator $G_\tau = \Psi e^{-\tau H}\Psi^{-1}$ and Readiness, the probability of being found in another regime at horizon τ. The graph Hamiltonian is unique given the data and the edge diffusivities, positive semidefinite and unitarily equivalent to a reversible Markov generator. Readiness has the spectral form $R_\tau = \sum_\ell B_\ell(1 - e^{-E_\ell \tau})$: a Bernstein function of the horizon whose asymptote is the Gini impurity of the regimes and whose initial slope is the probability flux across regime boundaries; only an observable part of the spectrum, generated by a Krylov subspace of the partition, contributes. Readiness is monotone under refinement of partitions, which gives a multiscale decomposition, bounds for joint regimes and a synchronization covariance that vanishes for separable systems. Reversibility is a likelihood-ratio test with b_1 degrees of freedom, the first Betti number of the state graph. The die is solved in closed form: its 26 levels split into six blocks of size at most three, one per irreducible representation of the octahedral group; the slowest modes form a random walk on the octahedron of faces, $E_1 = 2a/\sqrt{m}$ and $E_4 = 3a/\sqrt{m}$. We prove $nR_\infty \to 4$, $\sqrt{n}R_0' \to 8a$, the reciprocity law $E_1 E_{\mathrm{obs}} \to 2a\min(2a, 3b)$ and the gap law $E_6/E_5 = 2n/3 - 11/9 + O(1/n)$; spectral regime discovery returns the six outcomes, and crisp regimes reach exactly half of the spectral bound.

1. Introduction: the die that is ready to change

Throw a die and stop it in mid-air. Classical probability assigns it six equiprobable outcomes, or, if one is careful, a distribution over the 26 configurations on which a cube can rest: on a face, balanced on an edge, or poised on a vertex. That distribution answers the question *where is the die likely to be?* It does not answer the question one actually asks while the die is tumbling: *how likely is it to change what it shows within the next instant?* A die known to rest on one of six faces has Shannon entropy $\log 6$, the largest possible over the faces, and yet no propensity to change at all. Uncertainty is not readiness to change.

Quantum Data Statistics (QDS) [1, 2] was built to answer the second question. A distribution p is lifted to an amplitude $\psi = \sqrt{p}$; a Hamiltonian $H[p]$ is constructed whose ground state is exactly ψ; the propagator generated by H defines the canonical observable

$$R_\tau(b) = 1 - \sum_{j \in A_{r(b)}} G_\tau(j \mid b) = \mathbb{P}\big(r(X_{t+\tau}) \neq r(X_t) \mid X_t = b\big), \tag{1}$$

Readiness: the probability that the system will be found in a different regime after a horizon τ. In QDS Foundations the states are bins of a line and H is a second-difference operator. A die is not a line: its 26 configurations form a graph, faces touching edges and edges touching vertices, with

Date: 28 November 2026.

2020 *Mathematics Subject Classification.* Primary 60J27; Secondary 62M05, 05C50, 47A75, 62F03, 20C35.

Key words and phrases. Quantum Data Statistics, Readiness, graph Hamiltonian, reversible Markov processes, observable spectrum, Bernstein functions, metastability, multiscale partitions, likelihood ratio test, Betti number, octahedral symmetry, die.

the symmetry of the cube. The die therefore asks for QDS on a graph, and it turns out to be the ideal laboratory for it: every object can be written down, every theorem can be checked to machine precision, and the answers are often surprising.

This paper has four aims.

(1) **Preserve the canon.** Every definition of QDS Foundations is kept verbatim; only the spatial operator is generalised, from $-D_2$ to a weighted graph Laplacian (Section 2).
(2) **A spectral theory of Readiness.** Readiness is a positive superposition of relaxation modes, and only an *observable* part of the spectrum, selected by the partition, contributes (Sections 3–4).
(3) **A calculus of partitions and an inference.** Readiness is monotone under refinement, decomposes over scales, bounds joint regimes, measures synchronization, and the whole model is identifiable and falsifiable with a test whose degrees of freedom are topological (Sections 5–7).
(4) **Solve the die.** The 26-state cube is solved in closed form, its slow dynamics is identified as a random walk on the octahedron of faces, and the dynamics itself discovers the six outcomes (Section 8).

The main lesson is general: *the regimes one imposes by design (faces, edges, vertices) are not the regimes the dynamics creates (the six outcomes), and Readiness computed on the designed partition is blind to the slowest reorganization of the system.* The companion paper [3] carries the same machinery to markets, where the designed regimes are volatility, direction and dealer positioning.

Notation. $\mathcal{G} = (\mathcal{V}, \mathcal{E})$ is a finite, undirected, connected graph with $N = |\mathcal{V}|$; Δ_N° is the open simplex; for $p \in \Delta_N^\circ$, $\psi = \sqrt{p}$ and $\Psi = \mathrm{diag}(\psi)$. A partition $\mathcal{P} = \{A_1, \dots, A_K\}$ of $\mathcal{V}$ defines $r(i)$ (the regime of i), $P_r = \sum_{i \in A_r} p_i$ and the *regime amplitudes* $u_r = \mathbf{1}_{A_r} \odot \psi$. We use column-stochastic conventions: $G(j \mid i) = G_{ji}$, rates $q_{i \to j} = Q_{ji}$.

2. The QDS-G Hamiltonian

2.1. **Definition.** Let $D = (d_{ij})$ be symmetric with $d_{ii} = 0$, $d_{ij} \geq 0$ and $d_{ij} > 0 \iff \{i, j\} \in \mathcal{E}$: the *diffusivities* of the connections. Write $L_D = \mathrm{diag}(D\mathbf{1}) - D$ for the weighted Laplacian.

Definition 2.1 (QDS-G Hamiltonian)**.** For $p \in \Delta_N^\circ$,

$$H_{\mathcal{G}}[p] = L_D - \mathrm{diag}\Big(\frac{L_D\sqrt{p}}{\sqrt{p}}\Big), \qquad (H_{\mathcal{G}})_{ij} = \begin{cases} -d_{ij}, & i \neq j, \\ \displaystyle\sum_{k \neq i} d_{ik}\sqrt{p_k/p_i}, & i = j. \end{cases} \tag{2}$$

The potential $V_i = -(L_D\psi)_i/\psi_i$ is the discrete analogue of $D_2\sqrt{p}/\sqrt{p}$: it is determined by the data and is not a free parameter. On a path graph with unit diffusivities, (2) reduces to the canonical one-dimensional Hamiltonian of QDS Foundations up to the factor $\sigma^2/2$.

2.2. **Existence, uniqueness, positivity.**

Theorem 2.2 (Existence and uniqueness)**.** *Among real symmetric matrices with off-diagonal entries $-d_{ij}$, (2) is the unique one satisfying $H\sqrt{p} = 0$.*

Proof. $(H\psi)_i = H_{ii}\psi_i - \sum_{j \neq i} d_{ij}\psi_j$. Imposing $(H\psi)_i = 0$ fixes $H_{ii} = \sum_{j \neq i} d_{ij}\psi_j/\psi_i$, well defined because $\psi_i > 0$. □

Theorem 2.3 (Ground-state form and positivity)**.** *For every $f \in \mathbb{R}^N$,*

$$f^T H_{\mathcal{G}} f = \sum_{\{i,j\} \in \mathcal{E}} d_{ij}\,\psi_i\psi_j\Big(\frac{f_i}{\psi_i} - \frac{f_j}{\psi_j}\Big)^2. \tag{3}$$

Consequently $H_{\mathcal{G}} \succeq 0$ and, $\mathcal{G}$ being connected, $\ker H_{\mathcal{G}} = \mathrm{span}\{\sqrt{p}\}$*; the spectrum is $0 = E_0 < E_1 \leq \cdots \leq E_{N-1}$.*

Proof. $f^T H f = \sum_i H_{ii} f_i^2 - 2\sum_{i<j} d_{ij} f_i f_j = \sum_{i<j} d_{ij}\big(\frac{\psi_j}{\psi_i} f_i^2 + \frac{\psi_i}{\psi_j} f_j^2 - 2 f_i f_j\big)$, and the bracket equals $\psi_i\psi_j(f_i/\psi_i - f_j/\psi_j)^2$. Equality to zero forces $f_i/\psi_i = f_j/\psi_j$ on every edge, hence on all of $\mathcal{V}$. □

Formula (3) is the *ground-state representation*: in the variable $g = f/\psi$, H is the Dirichlet form of a random walk with edge conductances $c_{ij} = d_{ij}\sqrt{p_i p_j}$. These conductances, the *stationary edge fluxes*, will reappear in every result below.

2.3. **Stochastic equivalence.**

Theorem 2.4 (Reversible stochastic equivalence)**.** *Let $Q = -\Psi H_{\mathcal{G}} \Psi^{-1}$. Then $Q_{ij} = q_{j\to i} = d_{ij}\sqrt{p_i/p_j}$ for $i \neq j$, and*

$$\mathbf{1}^T Q = 0, \qquad Qp = 0, \qquad p_j\, q_{j\to i} = d_{ij}\sqrt{p_i p_j} = p_i\, q_{i\to j}.$$

Hence $G_\tau = e^{\tau Q} = \Psi e^{-\tau H_{\mathcal{G}}}\Psi^{-1}$ is a stochastic propagator with $G_\tau p = p$, $G_\tau \geq 0$ entrywise and $G_\tau \to p\mathbf{1}^T$; the levels E_ℓ are relaxation rates.

Proof. Column sums: $\sum_i Q_{ij} = \psi_j^{-1}\big(\sum_{i\neq j} d_{ij}\psi_i - H_{jj}\psi_j\big) = 0$ by Theorem 2.2. $Qp = -\Psi H\psi = 0$. Detailed balance follows from the symmetry of d. Positivity of $e^{\tau Q}$ holds because Q is a Metzler matrix. □

Corollary 2.5 (Identifiability)**.** *The map $(p, D) \mapsto Q$ is injective, with inverse*

$$d_{ij} = \sqrt{q_{j\to i}\, q_{i\to j}}, \qquad \frac{p_i}{p_j} = \frac{q_{j\to i}}{q_{i\to j}} \quad (\{i,j\} \in \mathcal{E}). \tag{4}$$

The QDS-G model has $\dim\Theta = |\mathcal{E}| + N - 1$ free parameters.

3. Canonical Readiness and its spectral representation

3.1. **Definition on graphs.**

For a partition $\mathcal{P}$ and horizon $\tau \geq 0$ we keep the canonical definitions

$$R_\tau(i) = 1 - \sum_{j\in A_{r(i)}} G_\tau(j \mid i), \qquad \widehat{R}_\tau = \operatorname{diag}\big(R_\tau(1), \ldots, R_\tau(N)\big), \qquad R_\tau(\rho) = \operatorname{Tr}(\rho\widehat{R}_\tau), \tag{5}$$

and the normalised index $\mathcal{R}_\tau = 100\, R_\tau(\rho)/\max_i R_\tau(i)$. Only the diagonal of ρ enters (5); for the stationary state we write ρ_p ($\operatorname{diag}\rho_p = p$). Whenever the dependence matters we write $R_\tau(H, p, \mathcal{P})$.

3.2. **The spectral theorem.**

Let $H_{\mathcal{G}}\phi_\ell = E_\ell\phi_\ell$ with an orthonormal eigenbasis, $\phi_0 = \psi$, and define the *participation coefficients*

$$B_\ell(\mathcal{P}) = \sum_{r=1}^{K} \langle u_r, \phi_\ell\rangle^2. \tag{6}$$

For degenerate levels we always sum B_ℓ over the eigenspace, which makes every statement basis-independent.

Theorem 3.1 (Spectral Readiness)**.**

$$R_\tau(\rho_p) = 1 - \sum_r \langle u_r, e^{-\tau H_{\mathcal{G}}} u_r\rangle = \sum_{\ell\geq 1} B_\ell(\mathcal{P})\big(1 - e^{-E_\ell\tau}\big), \qquad B_\ell \geq 0, \quad B_0 = \sum_r P_r^2, \quad \sum_{\ell\geq 0} B_\ell = 1. \tag{7}$$

Proof. By Theorem 2.4, $p_i G_\tau(j \mid i) = \psi_i\psi_j(e^{-\tau H})_{ji}$. Summing over $i, j \in A_r$ gives $\langle u_r, e^{-\tau H} u_r\rangle$, the stationary probability of starting and ending in A_r. Expanding in the eigenbasis, $\langle u_r, e^{-\tau H} u_r\rangle = \sum_\ell e^{-E_\ell\tau}\langle u_r, \phi_\ell\rangle^2$. For $\ell = 0$, $\langle u_r, \psi\rangle = P_r$. Parseval gives $\sum_\ell B_\ell = \sum_r \|u_r\|^2 = \sum_r P_r = 1$, and (7) follows. □

3.3. **First consequences.**

Corollary 3.2. *Let* $R_\infty = \lim_{\tau\to\infty} R_\tau(\rho_p)$ *and* $R'_0 = \partial_\tau R_\tau(\rho_p)|_{\tau=0}$.

(i) Equilibrium value. $R_\infty = \sum_{\ell\geq 1} B_\ell = 1 - \sum_r P_r^2 = 1 - e^{-H_2(P)}$*: the Gini impurity of the regime distribution (*H_2 *the Rényi-2 entropy).*

(ii) Bernstein property. $(-1)^{k+1}\partial_\tau^k R_\tau \geq 0$ *for all* $k \geq 1$*:* R_τ *is increasing, concave, and a Bernstein function of the horizon* [4].

(iii) Spectral sandwich. $R_\infty(1 - e^{-E_1\tau}) \leq R_\tau \leq R_\infty(1 - e^{-E_{N-1}\tau})$.

(iv) Boundary flux.

$$R'_0 = \sum_r \langle u_r, H_{\mathcal{G}} u_r\rangle = 2 \sum_{\{i,j\}\in\mathcal{E},\ r(i)\neq r(j)} d_{ij}\sqrt{p_i p_j} = 2\,\Phi(\mathcal{P}), \tag{8}$$

twice the stationary probability flux across regime boundaries. Edges internal to a regime do not contribute.

Proof. (i)–(iii) are immediate from (7). For (iv), differentiate (7) at 0 and apply (3) with $f = u_r$, for which $f_i/\psi_i = \mathbf{1}_{A_r}(i)$: an edge contributes $d_{ij}\psi_i\psi_j$ to $\langle u_r, Hu_r\rangle$ exactly when it leaves A_r, i.e. once for each of the two regimes it joins. □

For a non-stationary diagonal ρ the same differentiation of (5) gives the *infinitesimal Readiness*

$$\partial_\tau R_\tau(\rho)\big|_0 = \sum_i \rho_{ii} \sum_{j:\, r(j)\neq r(i)} q_{i\to j}, \tag{9}$$

the expected instantaneous rate of leaving the present regime. The quantity previously called "Dynamic Readiness", $\mathrm{Tr}(\rho\Gamma)$ with Γ the total exit rates, coincides with (9) only when every transition crosses a regime boundary, and should be called *Instantaneous Transition Intensity*. Similarly, $(\sum_i \sqrt{p_i})^2 - 1 = e^{H_{1/2}(p)} - 1$ is an *Effective Statistical Diversity* and $\frac{1}{2}\|\dot{p}\|_1$ a *Probability Redistribution Speed*; neither is Readiness.

3.4. **Normalised Readiness and the reorganization time.**

Definition 3.3. The *normalised Readiness* is $\widetilde{R}_\tau = R_\tau/R_\infty \in [0,1]$, and the *reorganization time* and *effective reorganization rate* are

$$T_R = \int_0^\infty \big(1 - \widetilde{R}_\tau\big)\, d\tau = \frac{1}{R_\infty}\sum_{\ell\geq 1}\frac{B_\ell}{E_\ell}, \qquad E_R = \frac{1}{T_R}. \tag{10}$$

Because $1 - \widetilde{R}_\tau = \sum_{\ell\geq 1} w_\ell e^{-E_\ell\tau}$ with $w_\ell = B_\ell/R_\infty$ summing to one, $\widetilde{R}_\tau$ is the distribution function of a mixture of exponential laws, and T_R is its mean: the expected time at which a regime change "happens", in the sense of the reorganization actually achieved.

Theorem 3.4 (Green representation and bounds for T_R)**.** *Let* $H_{\mathcal{G}}^+$ *be the Moore–Penrose inverse and* $\tilde{u}_r = u_r - P_r\psi$*. Then*

$$T_R = \frac{1}{R_\infty}\sum_r \langle \tilde{u}_r, H_{\mathcal{G}}^+ \tilde{u}_r\rangle, \tag{11}$$

and, with E_{obs} *and* $E_{\max}^{\mathrm{obs}}$ *the smallest and largest observable levels (Definition 4.1),*

$$\frac{1}{E_{\max}^{\mathrm{obs}}} \;\leq\; \frac{R_\infty}{R'_0} \;\leq\; T_R \;\leq\; \frac{1}{E_{\mathrm{obs}}}. \tag{12}$$

Proof. For $\ell \geq 1$, $\phi_\ell \perp \psi$, so $\langle u_r, \phi_\ell\rangle = \langle \tilde{u}_r, \phi_\ell\rangle$ and $\sum_{\ell\geq 1} B_\ell/E_\ell = \sum_r \langle \tilde{u}_r, H^+\tilde{u}_r\rangle$. In (12), the outer inequalities hold because T_R averages $1/E_\ell$ over observable levels; the middle one is Jensen's inequality for the convex map $x \mapsto 1/x$ under the weights w_ℓ: $\sum w_\ell E_\ell^{-1} \geq (\sum w_\ell E_\ell)^{-1} = R_\infty/R'_0$. □

Proposition 3.5 (Arithmetic and harmonic reorganization rates)**.** *Let $\Lambda_R = R_0'/R_\infty = \sum_\ell w_\ell E_\ell$ (weighted arithmetic mean of the observable rates) and $E_R = 1/T_R = (\sum_\ell w_\ell/E_\ell)^{-1}$ (weighted harmonic mean). Then*

$$E_{\mathrm{obs}} \le E_R \le \Lambda_R \le E_{\max}^{\mathrm{obs}}, \qquad \mathcal{H}_R := \Lambda_R T_R - 1 = \sum_{i<j} w_i w_j \frac{(E_i - E_j)^2}{E_i E_j} \ \ge 0. \tag{13}$$

Proof. Expand $(\sum_i w_i E_i)(\sum_j w_j/E_j) = \sum_i w_i^2 + \sum_{i\neq j} w_i w_j E_i/E_j$ and subtract $1 = (\sum w_i)^2$; each unordered pair contributes $w_i w_j(E_i/E_j + E_j/E_i - 2)$. □

The *spectral heterogeneity* $\mathcal{H}_R$ vanishes iff one level carries all observable weight; it measures how many distinct time scales a regime definition mixes. For the die at $n = 10$: $\mathcal{H}_R = 0.073$ for $\{C, A, V\}$ but 0.718 for the six face-basins (Section 6).

4. Observable spectrum

4.1. Invisible modes and the observable gap.

Definition 4.1. A level $E_\ell > 0$ is *invisible* for $\mathcal{P}$ if $B_\ell(\mathcal{P}) = 0$, i.e. $\langle u_r, \phi\rangle = 0$ for all r and every ϕ in its eigenspace. The *observable gap* is $E_{\mathrm{obs}}(\mathcal{P}) = \min\{E_\ell > 0 :\ B_\ell(\mathcal{P}) > 0\} \ge E_1$.

Theorem 4.2 (Observable relaxation)**.** *The Readiness deficit $\mathcal{D}_R(\tau) = R_\infty - R_\tau = \sum_{\ell\ge 1} B_\ell e^{-E_\ell \tau}$ is completely monotone and*

$$-\lim_{\tau\to\infty} \frac{1}{\tau} \log\big(R_\infty - R_\tau\big) = E_{\mathrm{obs}}(\mathcal{P}), \qquad \mathcal{D}_R(\tau) \sim B_{\mathrm{obs}}\, e^{-E_{\mathrm{obs}}\tau}.$$

Readiness relaxes at the observable gap, not at the spectral gap E_1. The global gap governs mixing of the whole state; Readiness only sees the part of the dynamics that crosses the chosen boundaries.

4.2. The Krylov reduction theorem.

Which modes are visible is decided by a finite-dimensional object.

Theorem 4.3 (Krylov reduction)**.** *Let $\mathcal{K}(\mathcal{P}) = \mathrm{span}\{H_{\mathcal{G}}^k u_r :\ k \ge 0,\ 1 \le r \le K\}$, the smallest $H_{\mathcal{G}}$-invariant subspace containing all regime amplitudes. Then:*

- *(a) $\psi \in \mathcal{K}$, and $R_\tau(\rho_p)$ depends on $H_{\mathcal{G}}$ only through its restriction $H_{\mathcal{K}} = H_{\mathcal{G}}|_{\mathcal{K}}$: if V is an orthonormal basis of $\mathcal{K}$, then $R_\tau(\rho_p) = 1 - \sum_r \langle V^T u_r, e^{-\tau V^T H_{\mathcal{G}} V} V^T u_r\rangle$.*
- *(b) The observable levels are exactly the nonzero eigenvalues of $H_{\mathcal{K}}$; every eigenvector in $\mathcal{K}^\perp$ is invisible. In particular the number of observable levels is at most $\dim\mathcal{K} - 1$.*

Proof. $\sum_r u_r = \psi$ gives $\psi \in \mathcal{K}$. Since H is symmetric, $\mathcal{K}$ and $\mathcal{K}^\perp$ are both invariant, so H has an eigenbasis adapted to $\mathcal{K} \oplus \mathcal{K}^\perp$. Each $u_r \in \mathcal{K}$ is orthogonal to eigenvectors in $\mathcal{K}^\perp$, which therefore have $B_\ell = 0$; and $e^{-\tau H} u_r = V e^{-\tau V^T H V} V^T u_r$. Conversely, a nonzero eigenvalue of $H_{\mathcal{K}}$ with $B_\ell = 0$ would have an eigenvector orthogonal to all u_r and hence, by invariance, to all $H^k u_r$, i.e. to $\mathcal{K}$ itself, a contradiction. □

Corollary 4.4 (Symmetry and invisibility)**.** *Let Γ be a group of permutations of $\mathcal{V}$ preserving D and p and leaving each regime A_r invariant. Then $\mathcal{K}(\mathcal{P}) \subseteq \mathrm{Fix}(\Gamma)$, $\dim \mathrm{Fix}(\Gamma)$ is the number of Γ-orbits, and every mode in a non-trivial isotypic component of Γ is invisible. Readiness can then be computed exactly on the quotient by orbits.*

Proof. Each u_r is Γ-invariant, and $\mathrm{Fix}(\Gamma)$ is H-invariant because the permutation matrices commute with H. The basis of normalised orbit indicators spans $\mathrm{Fix}(\Gamma)$. □

Theorem 4.3 turns the question "which reorganizations does my regime definition see?" into linear algebra: compute $\mathcal{K}(\mathcal{P})$. It also explains exactly why symmetric reductions of QDS are not approximations but identities.

5. A calculus of partitions

Readiness is a functional of the partition. Here no reversibility is needed unless stated: let (X_t) be any stationary Markov process on $\mathcal{V}$ with law p, and let $C_\tau(\mathcal{P}) = \{r_\mathcal{P}(X_t) \neq r_\mathcal{P}(X_{t+\tau})\}$, so $R_\tau(\mathcal{P}) = \mathbb{P}(C_\tau(\mathcal{P}))$.

5.1. Refinement monotonicity and multiscale decomposition.

Theorem 5.1 (Refinement)**.** *If $\mathcal{Q}$ refines $\mathcal{P}$ ($\mathcal{P} \preceq \mathcal{Q}$), then $C_\tau(\mathcal{P}) \subseteq C_\tau(\mathcal{Q})$ pathwise; hence $R_\tau(\mathcal{P}) \leq R_\tau(\mathcal{Q})$ for every τ and every initial law.*

Proof. States in different coarse regimes are in different fine regimes. □

For a chain $\mathcal{P}_0 \preceq \mathcal{P}_1 \preceq \cdots \preceq \mathcal{P}_L$ with $\mathcal{P}_0 = \{\mathcal{V}\}$ we obtain the *Multiscale Readiness Decomposition*

$$R_\tau(\mathcal{P}_L) = \sum_{k=1}^{L} \Delta R_\tau^{(k)}, \qquad \Delta R_\tau^{(k)} = R_\tau(\mathcal{P}_k) - R_\tau(\mathcal{P}_{k-1}) = \mathbb{P}\big(C_\tau(\mathcal{P}_k) \setminus C_\tau(\mathcal{P}_{k-1})\big) \geq 0, \tag{14}$$

the probability of reorganizations that are visible at scale k but invisible at all coarser scales.

Theorem 5.2 (Silent refinement)**.** *In QDS-G, if $\mathcal{Q}$ refines $\mathcal{P}$ and no edge of $\mathcal{G}$ joins two states lying in the same $\mathcal{P}$-regime but in different $\mathcal{Q}$-regimes, then $R'_0(\mathcal{Q}) = R'_0(\mathcal{P})$. The increment $\Delta R_\tau = R_\tau(\mathcal{Q}) - R_\tau(\mathcal{P})$ is then $O(\tau^2)$: it is produced entirely by multi-step, slow reorganization.*

Proof. By (8) both slopes are twice the flux across boundary edges, and the hypothesis says the two sets of boundary edges coincide. The same holds for (9) with arbitrary ρ. □

5.2. **Joint regimes: bounds and synchronization.** Let $\mathcal{P}^{(1)}, \ldots, \mathcal{P}^{(d)}$ be partitions (e.g. by volatility, direction, dealer flow) and $\mathcal{P}^\vee = \bigvee_k \mathcal{P}^{(k)}$ their common refinement. Since $C_\tau(\mathcal{P}^\vee) = \bigcup_k C_\tau(\mathcal{P}^{(k)})$,

$$\max_k R_\tau(\mathcal{P}^{(k)}) \;\leq\; R_\tau(\mathcal{P}^\vee) \;\leq\; \min\Big(1, \sum_k R_\tau(\mathcal{P}^{(k)})\Big). \tag{15}$$

Definition 5.3 (Reorganization synchronization)**.** For two partitions,

$$\mathcal{S}_\tau(\mathcal{P}, \mathcal{Q}) = R_\tau(\mathcal{P}) + R_\tau(\mathcal{Q}) - R_\tau(\mathcal{P} \vee \mathcal{Q}) - R_\tau(\mathcal{P})R_\tau(\mathcal{Q}) = \mathrm{Cov}\left(\mathbf{1}_{C_\tau(\mathcal{P})}, \mathbf{1}_{C_\tau(\mathcal{Q})}\right). \tag{16}$$

The identity follows from inclusion–exclusion. $\mathcal{S}_\tau > 0$ means that the two kinds of reorganization tend to happen together within the horizon; $\mathcal{S}_\tau < 0$ that one inhibits the other. As $\tau \to \infty$, $\mathcal{S}_\infty$ is the covariance of the change indicators for two independent draws from p: a *static* term that vanishes when the two labels are independent under p.

Theorem 5.4 (Separability)**.** *Let $\mathcal{G} = \mathcal{G}_1 \,\square\, \mathcal{G}_2$ be a Cartesian product graph, with diffusivities acting along each factor independently of the other coordinate ($D = D_1 \otimes I + I \otimes D_2$) and $p = p_1 \otimes p_2$. Then*

$$H_\mathcal{G}[p] = H_{\mathcal{G}_1}[p_1] \otimes I + I \otimes H_{\mathcal{G}_2}[p_2], \qquad G_\tau = G_\tau^{(1)} \otimes G_\tau^{(2)}. \tag{17}$$

The two coordinates are independent stationary processes; for any partitions $\mathcal{P}$ of the first factor and $\mathcal{Q}$ of the second, $\mathcal{S}_\tau(\mathcal{P}, \mathcal{Q}) \equiv 0$ and $1 - R_\tau(\mathcal{P} \vee \mathcal{Q}) = (1 - R_\tau(\mathcal{P}))(1 - R_\tau(\mathcal{Q}))$.

Proof. $L_D = L_{D_1} \otimes I + I \otimes L_{D_2}$ and $\psi = \psi_1 \otimes \psi_2$, so $(L_D\psi)/\psi = (L_{D_1}\psi_1/\psi_1) \otimes \mathbf{1} + \mathbf{1} \otimes (L_{D_2}\psi_2/\psi_2)$, which gives (17). Kronecker sums exponentiate to Kronecker products, and $\Psi = \Psi_1 \otimes \Psi_2$. □

Theorem 5.4 provides a null hypothesis: *reorganizations in different dimensions of a system are unsynchronized if and only if nothing couples them.* A non-zero $\mathcal{S}_\tau$ is evidence of coupling, through the distribution, through cross-diffusivities, or both.

6. Regime discovery

Readiness is computed on a partition. This section asks which partition the dynamics itself proposes.

6.1. **Spectral coordinates and the diffusion distance.** Let $f_\ell = \phi_\ell/\psi$ (componentwise). Then $\sum_i p_i f_\ell(i) f_k(i) = \delta_{\ell k}$ and $f_0 \equiv 1$: the f_ℓ are the right eigenfunctions of Q, orthonormal in $L^2(p)$. The propagator reads $G_\tau(k \mid i) = p_k \sum_\ell e^{-E_\ell \tau} f_\ell(k) f_\ell(i)$.

Theorem 6.1 (Diffusion distance)**.** *Define* $d_\tau^2(i,j) = \sum_k \big[G_\tau(k \mid i) - G_\tau(k \mid j)\big]^2/p_k$, *the* $L^2(1/p)$ *distance between the futures of* i *and* j. *Then*

$$d_\tau^2(i,j) = \sum_{\ell \geq 1} e^{-2E_\ell \tau} \big[f_\ell(i) - f_\ell(j)\big]^2. \tag{18}$$

Proof. The $\ell = 0$ term cancels since $f_0 \equiv 1$; orthonormality of $\{f_\ell\}$ in $L^2(p)$ removes the cross terms. □

This is the diffusion-map distance [8] written in QDS variables. Two states are dynamically close if their futures are; geometrically adjacent states may be dynamically far and conversely. At horizon τ, modes with $E_\ell \tau \gg 1$ are erased, so the spectral embedding $z_i^{(K)} = (f_1(i), \ldots, f_{K-1}(i))$ is the natural coordinate system for K regimes.

6.2. **How many regimes? Gap ratio, eigenspaces and heat trace.** Three diagnostics are used. (a) The *gap ratio* $\Gamma_K = E_K/E_{K-1}$, with $K^* = \arg\max_K \Gamma_K$. (b) The *degeneracy rule*: a candidate K is admissible only if $E_K > E_{K-1}$, since a degenerate eigenspace has no preferred basis and only its projector $\Pi_E = \sum_{E_\ell = E} \phi_\ell \phi_\ell^T$ is meaningful; cutting through it makes regimes basis-dependent. (c) The *heat trace*

$$N_{\text{eff}}(\tau) = \operatorname{Tr} e^{-\tau H_{\mathcal{G}}} = \sum_\ell e^{-E_\ell \tau}, \qquad N_{\text{eff}}(0) = N, \quad N_{\text{eff}}(\infty) = 1, \tag{19}$$

the effective number of dynamical degrees of freedom alive at horizon τ; a plateau $N_{\text{eff}} \approx K$ over a range of horizons signals K metastable regimes, without reference to a single ratio.

6.3. **A variational bound for regime quality.** For $\mathcal{P}$ with $P_r > 0$ set $v_r = u_r/\sqrt{P_r}$; these are orthonormal, and by (3) $v_r^T H_{\mathcal{G}} v_r = \operatorname{cut}(A_r)/P_r$, where $\operatorname{cut}(A_r) = \sum_{i \in A_r,\, j \notin A_r} d_{ij}\sqrt{p_i p_j}$.

Theorem 6.2 (Ky Fan bound)**.** *For every partition into* K *regimes,*

$$J_K(\mathcal{P}) = \sum_{r=1}^{K} \frac{\operatorname{cut}(A_r)}{P_r} \;\geq\; \sum_{\ell=1}^{K-1} E_\ell, \qquad \eta(\mathcal{P}) = \frac{\sum_{\ell=1}^{K-1} E_\ell}{J_K(\mathcal{P})} \in (0,1]. \tag{20}$$

Proof. $J_K = \operatorname{Tr}(V^T H_{\mathcal{G}} V)$ with $V = [v_1, \ldots, v_K]$, $V^T V = I_K$; Ky Fan's principle gives $\operatorname{Tr}(V^T H V) \geq \sum_{\ell < K} E_\ell$, and $E_0 = 0$. □

J_K is the normalised cut of spectral clustering; η is the *spectral efficiency* of a regime definition. Equation (8) shows $\sum_r \operatorname{cut}(A_r) = R_0'$, so J_K is a mass-weighted version of the initial Readiness slope. Bipartitions give $E_1 \leq R_0'/R_\infty$, and in general $R_0' \geq E_{\text{obs}} R_\infty \geq E_1 R_\infty$; the converse is Cheeger's inequality for reversible chains [5].

Fuzzy regimes. If the K slowest eigenfunctions are mapped linearly onto memberships $\chi_r(i) \geq 0$, $\sum_r \chi_r = 1$ (PCCA [6]), the fuzzy regime amplitudes $w_r = \psi \odot \chi_r$ span exactly the slow eigenspace, and the generalised objective $\operatorname{Tr}\big((W^T W)^{-1} W^T H_{\mathcal{G}} W\big)$ equals $\sum_{\ell < K} E_\ell$: *fuzzy regimes attain the bound,* $\eta = 1$. Crisp regimes cannot, whenever transition states exist (Theorem 8.8).

7. QDS-G as an inferential statistics

7.1. **Likelihood and sufficient statistics.** Suppose a trajectory of the QDS-G process is observed on $[0,T]$. Let $N_{i\to j}$ be the number of jumps $i\to j$ and h_i the time spent in i. The log-likelihood of a continuous-time chain with rates q is

$$\ell(q)=\sum_{i\neq j}\big(N_{i\to j}\log q_{i\to j}-h_i\,q_{i\to j}\big), \tag{21}$$

so (N,h) is sufficient. The unrestricted MLE is $\hat q_{i\to j}=N_{i\to j}/h_i$. Substituting into (4) gives the plug-in QDS-G estimators

$$\hat d_{ij}=\sqrt{\frac{N_{i\to j}N_{j\to i}}{h_ih_j}},\qquad \hat p_i\propto h_i,\qquad \widehat H=H_{\mathcal G}[\hat p]\text{ with }\hat D,\qquad \widehat R_\tau=R_\tau(\widehat H,\hat p,\mathcal P). \tag{22}$$

Proposition 7.1 (Consistency and asymptotic variance)**.** *If the process is ergodic, $\hat d_{ij}\to d_{ij}$ and $\widehat R_\tau\to R_\tau$ almost surely as $T\to\infty$, and by the delta method*

$$\operatorname{Var}\big(\log\hat d_{ij}\big)\simeq\frac14\Big(\frac{1}{N_{i\to j}}+\frac{1}{N_{j\to i}}\Big). \tag{23}$$

Proof. $\hat q$ is consistent with $\operatorname{Var}(\log\hat q_{i\to j})\simeq 1/N_{i\to j}$, and the estimators for the two directions are asymptotically independent; $\log\hat d=\frac12(\log\hat q_{i\to j}+\log\hat q_{j\to i})$. R_τ is a continuous function of (p,D). □

7.2. **Testing reversibility: a test with topological degrees of freedom.** QDS-G is a strict submodel of the general Markov chain on $\mathcal G$. Its validity is testable.

Theorem 7.2 (Reversibility test)**.** *On a connected graph $\mathcal G$, the general chain with independent rates in both directions of every edge has $2|\mathcal E|$ parameters, and QDS-G has $|\mathcal E|+|\mathcal V|-1$. The difference is the first Betti number*

$$2|\mathcal E|-\big(|\mathcal E|+|\mathcal V|-1\big)=|\mathcal E|-|\mathcal V|+1=b_1(\mathcal G). \tag{24}$$

Hence, under regularity conditions and when QDS-G holds, the likelihood-ratio statistic $\Lambda=2\big(\sup\ell-\sup_{\text{QDS-G}}\ell\big)$ is asymptotically $\chi^2_{b_1(\mathcal G)}$ (Wilks [11]). The b_1 restrictions are Kolmogorov's criterion: the cycle affinities $\mathcal A_c=\log\prod_{e\in c}q_e^+/q_e^-$ vanish on a basis of the cycle space.

Proof. The parameter count follows from Corollary 2.5. A chain on $\mathcal G$ is reversible iff its affinities vanish on every cycle (Kolmogorov), and it suffices to impose this on a cycle basis [10], which has b_1 elements; the constraints are independent because the cycle-space coordinates of $\log(q^+/q^-)$ are free in the general model. □

The cycles of the state graph, introduced in the original research plan as phase-consistency conditions, thus reappear as the degrees of freedom of a test: $b_1=23$ for the incidence graph of the die and $b_1=47$ for its Voronoi graph. Rejection means that the system carries probability currents around cycles, which no QDS-G Hamiltonian can generate, and calls for a non-reversible extension.

8. The cubic die: an exactly solvable QDS-G system

8.1. **States, graphs and data.** The 26 geometric states are $\mathcal V=\{-1,0,1\}^3\setminus\{0\}$, classified by $k(s)=|x|+|y|+|z|$: 6 faces (C), 12 edges (A), 8 vertices (V). The *incidence graph* joins a face to its 4 edges and an edge to its 2 vertices: $|\mathcal E|=48$, $b_1=23$. A physical orientation is classified by the nearest of the 26 unit directions; the induced spherical Voronoi tessellation has **72** adjacencies, because each kite face–edge–vertex–edge splits along its shorter diagonal (face–vertex $54.74^\circ<$ edge–edge 60°). We work with the incidence graph and check every result on the Voronoi graph with an extra face–vertex diffusivity c (Figure 1).

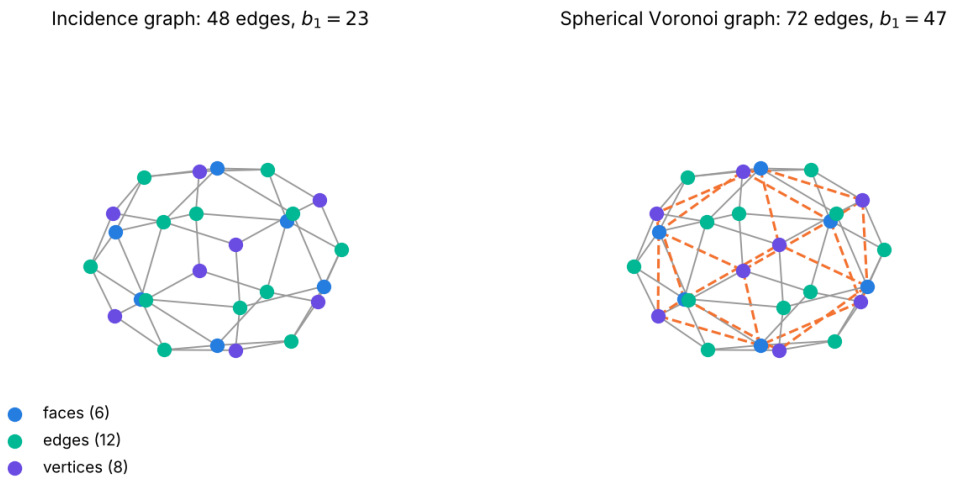

FIGURE 1. The two state graphs of the die on the unit sphere. Dashed: the 24 face–vertex adjacencies of the orientation (Voronoi) graph.

As a reference distribution we take the uniform surface lattice with n points per cube edge, $m = n - 2$, $M = 6n^2 - 12n + 8$ points, giving per-state weights $p_c : p_a : p_v = m^2 : m : 1$ and

$$P_C = \frac{6m^2}{M} = 1 - \frac{2}{n} + O(n^{-2}), \qquad P_A = \frac{12m}{M} \sim \frac{2}{n}, \qquad P_V = \frac{8}{M} \sim \frac{4}{3n^2}. \tag{25}$$

Diffusivities are a on face–edge and b on edge–vertex connections. The 488-point lattice ($n = 10$) has isotropic inertia $I_0 = \frac{ma^2}{6(n-1)}[n^3(n+1) - (n-2)^3(n-3)]$, $I_0/(Ma^2) \to 5/18$; this is relevant for the physical simulator, not for QDS-G.

8.2. **Exact reduction of the geometric Readiness.** The octahedral group O_h (order 48) preserves D, p and each of C, A, V. By Corollary 4.4, Readiness for $\mathcal{P}_2 = \{C, A, V\}$ lives on $\mathrm{Fix}(O_h) = \mathrm{span}\{|C\rangle, |A\rangle, |V\rangle\}$ (normalised orbit sums), where

$$H_{\mathrm{red}} = \begin{pmatrix} \frac{4a}{\sqrt{m}} & -2\sqrt{2}\,a & 0 \\ -2\sqrt{2}\,a & 2a\sqrt{m} + \frac{2b}{\sqrt{m}} & -\sqrt{6}\,b \\ 0 & -\sqrt{6}\,b & 3b\sqrt{m} \end{pmatrix}, \qquad \det H_{\mathrm{red}} = 0, \tag{26}$$

with trace T, second invariant $B = ab(6m + 12 + 8/m)$ and visible levels $E_\pm = \frac{1}{2}(T \pm \sqrt{T^2 - 4B})$. (On the Voronoi graph add $4c/m$, $3cm$ to the diagonal and $-2\sqrt{3}\,c$ to the (C, V) entries.) $\mathcal{K}(\mathcal{P}_2)$ is three-dimensional: **23 of the 26 dimensions are invisible to the geometric Readiness**.

Corollary 8.1 (Explicit Readiness of the die)**.** *Let $\phi_\pm = (\phi_\pm(C), \phi_\pm(A), \phi_\pm(V))$ be the normalised eigenvectors of H_{red} for $E_\pm$. Since the regime amplitudes are $u_r = \sqrt{P_r}\,|r\rangle$ in the orbit basis,*

$$B_\pm = \sum_{r \in \{C,A,V\}} P_r\,\phi_\pm(r)^2, \qquad R_\tau = B_-\big(1 - e^{-E_-\tau}\big) + B_+\big(1 - e^{-E_+\tau}\big), \tag{27}$$

and the ground state of H_{red} is $(\sqrt{P_C}, \sqrt{P_A}, \sqrt{P_V})$.

Proof. $\langle u_r, \phi\rangle = \sqrt{P_r}\,\phi(r)$ for every ϕ in $\mathrm{Fix}(O_h)$; substitute in (6). The ground state is ψ written in the orbit basis. □

Example 8.2 ($n = 10$, $a = b = 1$)**.** $T = 16.263456$, $B = 61$, $E_- = 5.867882$, $E_+ = 10.395574$, and

$$R_\tau = 0.231864\,\big(1 - e^{-5.867882\,\tau}\big) + 0.109980\,\big(1 - e^{-10.395574\,\tau}\big),$$

$R_\infty = 0.341844 = 1 - (384^2 + 96^2 + 8^2)/488^2$, $R_0' = 2.503854 = 432\sqrt{8}/488$, $T_R = 0.146539$, $E_R = 6.8241$, $J = 1.073$.

8.3. **A worked example: the 488-point die, step by step.** We follow every step for the uniform lattice with $n = 10$ points per edge (488 points) and $a = b = 1$.

(1) *Data.* $m = 8$; per-state probabilities $p_c = 64/488$, $p_a = 8/488$, $p_v = 1/488$; regime masses $P = (P_C, P_A, P_V) = (384, 96, 8)/488 = (0.7869, 0.1967, 0.0164)$.

(2) *Amplitude.* $\psi_c : \psi_a : \psi_v = 8 : 2\sqrt{2} : 1$; in the orbit basis $\sqrt{P} = (0.887066, 0.443533, 0.128037)$.

(3) *Hamiltonian.* The diagonal entries are $h_C = 4/\sqrt{8} = 1.414214$, $h_A = 2\sqrt{8} + 2/\sqrt{8} = 6.363961$, $h_V = 3\sqrt{8} = 8.485281$: each state "feels" the amplitude of its neighbours relative to its own, so faces, which dominate their neighbourhood, have the smallest potential. In the orbit basis

$$H_{\text{red}} = \begin{pmatrix} 1.414214 & -2.828427 & 0 \\ -2.828427 & 6.363961 & -2.449490 \\ 0 & -2.449490 & 8.485281 \end{pmatrix}, \qquad H_{\text{red}}\sqrt{P} = 0.$$

(4) *Spectrum.* $E_0 = 0$, $E_- = 5.867882$, $E_+ = 10.395574$, with eigenvectors

$$\phi_- = (0.4207, -0.6624, -0.6199), \qquad \phi_+ = (0.1901, -0.6038, 0.7742).$$

(5) *Participation.* By (27): $B_0 = \sum_r P_r^2 = 0.658156$, $B_- = 0.231864$, $B_+ = 0.109980$, and $B_0 + B_- + B_+ = 1$.

(6) *Readiness.* $R_\tau = 0.231864(1 - e^{-5.867882\tau}) + 0.109980(1 - e^{-10.395574\tau})$, so $R_{0.1} = 0.17401$, $R_{0.5} = 0.32890$, $R_1 = 0.34118$, $R_\infty = 0.341844$. One third of the stationary probability will, eventually, be found in another geometric class.

(7) *Time scales.* $R_0' = 2.503854$ (boundary flux), $T_R = 0.146539$, $E_R = 6.8241$, $\mathcal{H}_R = 0.073$: a single dominant time scale.

(8) *The slow modes the geometric Readiness does not see.* The full 26×26 spectrum has $E_1 = 0.646105$ (threefold) and $E_4 = 1.038649$ (twofold). The octahedral rate (29) gives $k = 0.157135$, $4k = 0.6285$ and $6k = 0.9428$, already within 3% and 10% at this small n. These modes move probability between faces; the partition $\{C, A, V\}$ cannot see them because it does not distinguish one face from another.

8.4. **The full spectrum: three clusters.**

Theorem 8.3 (Spectral structure of the die)**.** *Fix $a, b > 0$ with $2a \neq 3b$. As $m \to \infty$ the 26 levels of $H_{\mathcal{G}}$ split into*

$$\underbrace{\{0\} \cup \left\{\tfrac{2a}{\sqrt{m}}\right\}^{(3)} \cup \left\{\tfrac{3a}{\sqrt{m}}\right\}^{(2)}}_{\text{slow octahedral sector}} \cup \underbrace{\{2a\sqrt{m} + O(1)\}^{(12)}}_{\text{edge cluster}} \cup \underbrace{\{3b\sqrt{m} + O(1)\}^{(8)}}_{\text{vertex cluster}} \quad (1 + o(1)), \tag{28}$$

and the slow sector is, to leading order, the Laplacian of a continuous-time random walk on the octahedron (faces as nodes) with rate

$$k = \frac{a}{\sqrt{m}} \cdot \frac{a\sqrt{m}}{2a\sqrt{m} + 2b/\sqrt{m}} = \frac{a}{2\sqrt{m}}\Big(1 + \frac{b}{am}\Big)^{-1}. \tag{29}$$

Proof sketch. Write $H = \sqrt{m}\, H^{(1)} + H^{(0)} + m^{-1/2} H^{(-1)}$. The leading part is diagonal: 0 on faces, $2a$ on edges, $3b$ on vertices; this yields the two fast clusters with multiplicities 12 and 8. On the six-dimensional face space, the Schur complement (Feshbach map) of the fast block gives the effective operator

$$H_{\text{eff}} = \frac{4a}{\sqrt{m}} I_6 - \frac{a^2}{2a\sqrt{m}}\, \mathsf{B}\mathsf{B}^T + o(m^{-1/2}),$$

where B is the 6×12 face–edge incidence matrix. Since each face has four edges and two faces share at most one edge, $\mathsf{B}\mathsf{B}^T = 4I + \mathsf{A}_{\mathrm{oct}}$ with $\mathsf{A}_{\mathrm{oct}}$ the adjacency of the octahedron. Hence $H_{\mathrm{eff}} = \frac{a}{2\sqrt{m}}(4I - \mathsf{A}_{\mathrm{oct}}) = k\, L_{\mathrm{oct}}$, whose spectrum $\{0, 4k^{(3)}, 6k^{(2)}\}$ corresponds to the decomposition $A_{1g} \oplus T_{1u} \oplus E_g$ of the permutation representation of O_h on the faces. The factor in (29) is the probability that an excursion into an edge returns to a face rather than continuing to a vertex. □

Numerically (Table 1, Figure 3), $\sqrt{m}E_1 = 2.0000$ and $\sqrt{m}E_4 = 3.0000$ at $n = 10^5$ for every (a, b) tested, and the fast levels divided by $\sqrt{m}$ cluster at $2a$ (12 levels) and $3b$ (8 levels).

Corollary 8.4 (Visible levels and reciprocity)**.** *The two observable levels of the geometric Readiness are the symmetric representatives of the fast clusters:*

$$\frac{E_-}{\sqrt{m}} \to \min(2a, 3b), \qquad \frac{E_+}{\sqrt{m}} \to \max(2a, 3b), \tag{30}$$

because $T^2 - 4B = (2a - 3b)^2 m + O(1)$. *Consequently the observable and global gaps obey the* reciprocity law

$$E_1 \cdot E_{\mathrm{obs}} \;\longrightarrow\; 2a \cdot \min(2a, 3b), \qquad \frac{E_{\mathrm{obs}}}{E_1} \sim \frac{\min(2a, 3b)}{2a}\, m. \tag{31}$$

For $n = 10$, $a = b = 1$: $E_1 = 0.646105$, $E_{\mathrm{obs}} = 5.867882$, ratio 9.08; the geometric Readiness relaxes nine times faster than the slowest reorganization of the die.

8.5. **The complete analytic spectrum via irreducible representations.** The permutation representations of O_h on faces, edges and vertices decompose as

$$\text{faces} = A_{1g} \oplus E_g \oplus T_{1u}, \quad \text{edges} = A_{1g} \oplus E_g \oplus T_{1u} \oplus T_{2g} \oplus T_{2u}, \quad \text{vertices} = A_{1g} \oplus A_{2u} \oplus T_{1u} \oplus T_{2g}.$$

Since $H_{\mathcal{G}}$ commutes with O_h, it is block-diagonal by irreducible representation, each block of size equal to the number of orbits containing that irrep. With $s = \sqrt{m}$, $h_C = 4a/s$, $h_A = 2as + 2b/s$, $h_V = 3bs$ (the common diagonal on each orbit), and the singular values of the face–edge incidence ($\sqrt{8}, \sqrt{2}, 2$ on A_{1g}, E_g, T_{1u}, from $\mathsf{B}\mathsf{B}^T = 4I + \mathsf{A}_{\mathrm{oct}}$) and of the edge–vertex incidence ($\sqrt{6}, 2, \sqrt{2}, 0$ on $A_{1g}, T_{1u}, T_{2g}, A_{2u}$, from $\mathsf{C}^T\mathsf{C} = 3I + \mathsf{A}_{\mathrm{cube}}$):

Theorem 8.5 (Exact spectrum of the cubic die)**.** *The 26 eigenvalues of $H_{\mathcal{G}}$ are the eigenvalues of*

$$A_{1g}\ (\times 1):\ \begin{pmatrix} h_C & -2\sqrt{2}a & 0 \\ -2\sqrt{2}a & h_A & -\sqrt{6}b \\ 0 & -\sqrt{6}b & h_V \end{pmatrix}, \quad T_{1u}\ (\times 3):\ \begin{pmatrix} h_C & -2a & 0 \\ -2a & h_A & -2b \\ 0 & -2b & h_V \end{pmatrix},$$

$$E_g\ (\times 2):\ \begin{pmatrix} h_C & -\sqrt{2}a \\ -\sqrt{2}a & h_A \end{pmatrix}, \quad T_{2g}\ (\times 3):\ \begin{pmatrix} h_A & -\sqrt{2}b \\ -\sqrt{2}b & h_V \end{pmatrix}, \quad T_{2u}\ (\times 3):\ h_A, \quad A_{2u}\ (\times 1):\ h_V.$$

Counting dimensions: $3{+}3{\cdot}3{+}2{\cdot}2{+}3{\cdot}2{+}3{+}1 = 26$, and there are exactly 12 distinct levels. The decomposition agrees with direct diagonalisation to 2×10^{-15} (relative) over 200 random (n, a, b). Every spectral quantity of the die is therefore given by roots of polynomials of degree at most three: the 26-state problem is solved in closed form. Figure 2 shows the twelve levels as functions of n, coloured by representation. Two levels are explicit, $h_A = 2a\sqrt{m} + 2b/\sqrt{m}$ (edge modes antisymmetric under inversion that couple to nothing) and $h_V = 3b\sqrt{m}$ (the alternating vertex mode).

Theorem 8.6 (Six-regime gap law)**.** *Let $2a < 3b$. The fifth nonzero level is the small root of the E_g block,*

$$E_5 = \frac{3a}{\sqrt{m}} + \Big(b - \frac{3a}{2}\Big) m^{-3/2} + O(m^{-5/2}), \tag{32}$$

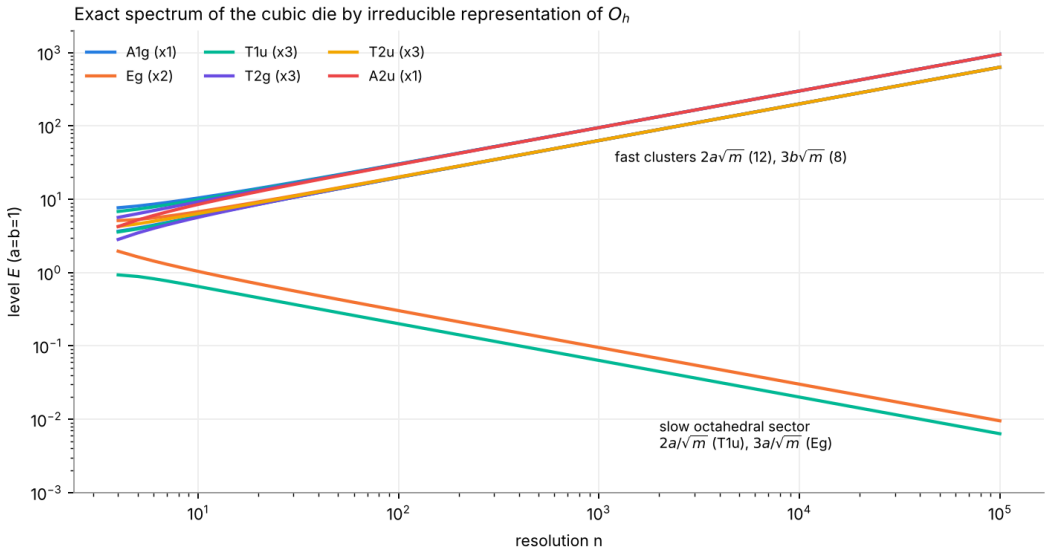

FIGURE 2. The exact spectrum of the cubic die, $a = b = 1$: the twelve distinct levels of the six irreducible blocks of Theorem 8.5 (multiplicities in brackets). The slow sector (T_{1u} and E_g small roots, together with 0 in A_{1g}) separates from the fast clusters as n grows.

the sixth is $E_6 = 2a\sqrt{m} + \kappa\, m^{-1/2} + O(m^{-3/2})$ *with*

$$\kappa = \min\left\{2b - \tfrac{2b^2}{3b-2a},\ 2a + 2b - \tfrac{4b^2}{3b-2a},\ 4a + 2b - \tfrac{6b^2}{3b-2a},\ 2b,\ a + 2b\right\}$$

(the middle roots of T_{2g}, T_{1u}, A_{1g} *and the levels* T_{2u}*, upper* E_g*), and*

$$\Gamma_6 = \frac{E_6}{E_5} = \frac{2m}{3} + \frac{\kappa}{3a} - \frac{2b}{9a} + \frac{1}{3} + O(m^{-1}). \tag{33}$$

For $a = b = 1$*,* $\kappa = 0$ *and* $\Gamma_6 = \frac{2n}{3} - \frac{11}{9} + O(n^{-1})$*. If* $3b < 2a$ *the leading term becomes* $\Gamma_6 \sim bm/a$ *(the first fast level is then the symmetric vertex mode).*

Proof. For the E_g block, with $\Delta = h_A - h_C = 2as + (2b-4a)/s$, the small root is $h_C - \frac{2a^2}{\Delta} + \frac{4a^4}{\Delta^3} + \ldots$; expanding $1/\Delta$ in s^{-2} gives (32). For the fast levels near h_A, second-order perturbation within each block gives $h_A + \sum_{\text{couplings}} g^2/(h_A - h_X)$ with $h_A - h_C \simeq 2as$ and $h_A - h_V \simeq (2a - 3b)s$, which yields the five candidates for κ. Dividing and expanding, $(2s + \kappa/(as)) \cdot \frac{s}{3}\big(1 - \frac{b-3a/2}{3as^2}\big)$ gives (33). □

Numerically, $\Gamma_6 - 2m/3$ equals 0.111111 ($a = b = 1$, predicted 1/9), 0.555552 ($a = 1, b = 2$, predicted 5/9) and 0.399997 ($a = 2, b = 3$, predicted 2/5) at $m = 10^5$; for $a = b = 1$, $\Gamma_6(n) = 12.1121, 32.1115, 65.4446, 665.4445$ at $n = 20, 50, 100, 1000$ against $2n/3 - 11/9 = 12.1111, 32.1111, 65.4444, 665.4444$. The sixth level is the T_{2g} edge–vertex mode when $2a < 3b$ and the symmetric A_{1g} mode otherwise.

8.6. **Asymptotic laws.**

n	E_1	E_{obs}	$E_1 E_{\text{obs}}$	nR_∞	$\sqrt{n}R'_0$	T_R	$2a\sqrt{m}\,T_R$
3	0.858664	3.438447	2.952	1.917160	6.395265	0.200850	0.4017
10	0.646105	5.867882	3.791	3.418436	7.917880	0.146539	0.8290
100	0.200652	19.806766	3.974	3.946137	7.999320	0.049710	0.9843
10^3	0.063267	63.182528	3.997	3.994661	7.999993	0.015799	0.9984
10^4	0.020001	199.980007	4.000	3.999467	8.000000	0.005000	0.9998
10^6	0.002000	1999.998	4.000	3.999995	8.000000	0.000500	1.0000

TABLE 1. Exact numerical values for $a = b = 1$, incidence graph. Limits: $E_1 E_{\text{obs}} \to 4$, $nR_\infty \to 4$, $\sqrt{n}R'_0 \to 8$, $2a\sqrt{m}\,T_R \to 1$. For $(a, b) = (1, 0.3)$ the reciprocity limit is 1.8000, as predicted by (31).

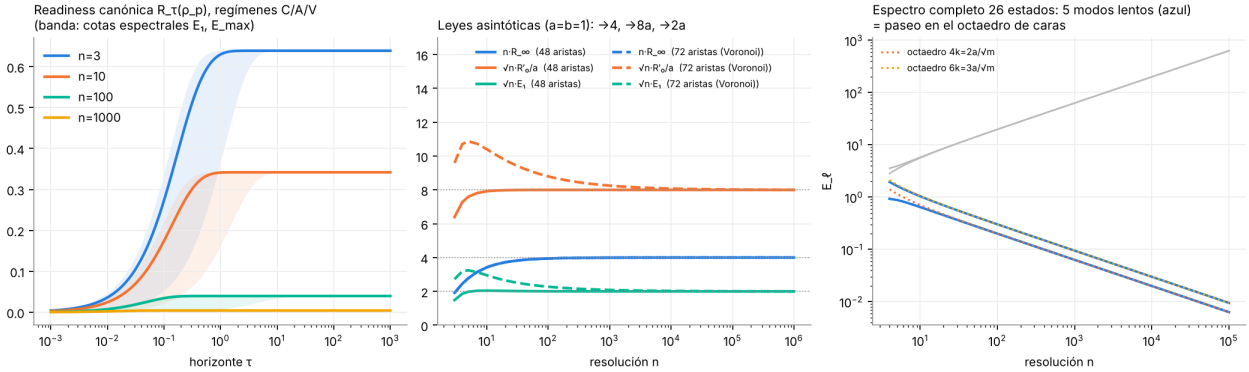

FIGURE 3. Left: geometric Readiness $R_\tau(\rho_p)$ for four resolutions with the spectral sandwich of Corollary 3.2(iii). Centre: the laws $nR_\infty \to 4$, $\sqrt{n}R'_0/a \to 8$, $\sqrt{n}E_1 \to 2a$ on both graphs. Right: full spectrum; the five slow levels (blue) follow $2a/\sqrt{m}$ and $3a/\sqrt{m}$.

Theorem 8.7 (Readiness laws of the die)**.** *For the partition $\{C, A, V\}$, as $n \to \infty$ with a, b fixed:*

$$R_\infty(n) = 1 - \frac{36(n-2)^4 + 144(n-2)^2 + 64}{(6n^2 - 12n + 8)^2} \sim \frac{4}{n}, \tag{34}$$

$$R'_0(n) = \frac{48\sqrt{n-2}\,[a(n-2) + b]}{6n^2 - 12n + 8} \sim \frac{8a}{\sqrt{n}}, \tag{35}$$

$$T_R(n) \sim \frac{1}{2a\sqrt{m}} \qquad \textit{(independent of } b\textit{)}, \tag{36}$$

and $J = T_R R'_0 / R_\infty \to 1$: asymptotically all observable weight sits on the edge-cluster mode.

Proof. (34) is Corollary 3.2(i) with (25); (35) is (8) with 24 face–edge and 24 edge–vertex boundary edges, $\sqrt{p_c p_a} = m^{3/2}/M$, $\sqrt{p_a p_v} = m^{1/2}/M$. For (36), R_∞ is dominated by the face–edge mixing $2P_C P_A$, whose relaxation is carried by the symmetric edge mode of rate $2a\sqrt{m}$; the vertex mode carries weight $O(P_V) = O(n^{-2})$. Then $T_R \approx R_\infty^{-1} \cdot R_\infty/(2a\sqrt{m})$. □

Law (36) contains a subtle point. When $3b < 2a$, the observable gap is the *vertex* mode $3b\sqrt{m}$, but its weight vanishes like n^{-2}; the asymptotic decay rate of the deficit (Theorem 4.2) is then set by a mode that carries almost no reorganization. $E_R = 1/T_R$ is the operationally relevant rate and is unaffected (Figure 4, left: for $b = 0.3$, $E_{\text{obs}} \approx 0.9\sqrt{m}$ while $E_R \approx 2\sqrt{m}$). On the Voronoi graph, R_∞ is unchanged and R'_0 gains $48c\,m/M \sim 8c/n$, subleading to (35).

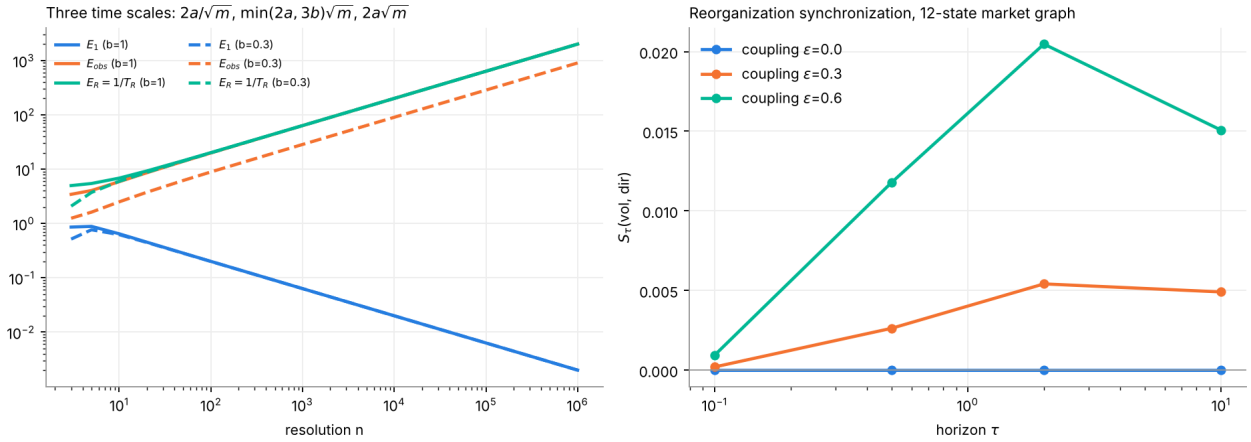

FIGURE 4. Left: the three time scales of the die, $E_1 \sim 2a/\sqrt{m}$, $E_{\text{obs}} \sim \min(2a, 3b)\sqrt{m}$ and $E_R \sim 2a\sqrt{m}$, for $b = 1$ (solid; E_{obs} and E_R coincide) and $b = 0.3$ (dashed). Right: reorganization synchronization between volatility and direction on the 12-state market graph; $\mathcal{S}_\tau \equiv 0$ for the separable model, as Theorem 5.4 requires.

8.7. **Multiscale Readiness: what the geometric regimes miss.** Consider the nested partitions $\mathcal{P}_1 = \{C, \neg C\} \preceq \mathcal{P}_2 = \{C, A, V\} \preceq \mathcal{P}_3 = \{c_1, \ldots, c_6, A, V\} \preceq \mathcal{P}_4 =$ singletons. Table 2 and Figure 5 show the result for $n = 10$, $a = b = 1$.

Partition	K	$\dim \mathcal{K}$	obs. levels	E_{obs}	R_∞	R'_0
$\mathcal{P}_1$: C | not C	2	3	2	5.8679	0.335394	2.225648
$\mathcal{P}_2$: C / A / V	3	3	2	5.8679	0.341844	2.503854
$\mathcal{P}_3$: 6 faces / A / V	8	16	7	0.6461	0.857834	2.503854
$\mathcal{P}_4$: 26 singletons	26	26	11	0.6461	0.893543	2.503854

TABLE 2. Multiscale Readiness of the die ($n = 10$, $a = b = 1$). Refinement $\mathcal{P}_2 \to \mathcal{P}_3 \to \mathcal{P}_4$ is silent (Theorem 5.2): R'_0 does not change, yet R_∞ jumps from 0.34 to 0.86.

The refinement $\mathcal{P}_2 \to \mathcal{P}_3$ adds no boundary edge (faces are never adjacent), so by Theorem 5.2 the extra Readiness $\Delta R_\tau^{(3)}$ has zero initial slope; yet it carries 0.516 of probability: *more than half of all reorganization of the die is a slow change of outcome that the geometric regimes cannot see.* Its relaxation is governed by the octahedral sector, $E_{\text{obs}}(\mathcal{P}_3) = E_1$, and Theorem 8.3 gives its closed form: for the face-to-face transfer,

$$R_\tau^{\text{face}} = \frac{5}{6} - \frac{1}{2}e^{-4k\tau} - \frac{1}{3}e^{-6k\tau}, \tag{37}$$

which agrees with the full propagator to 7×10^{-4} at $n = 10^3$ and 7×10^{-6} at $n = 10^5$.

8.8. **Regime discovery on the die.**
Number of regimes. Applying the gap-ratio rule with the degeneracy constraint over $K \in \{2, \ldots, 8\}$ to the grid $n \in \{3, 5, 10, 20, 50, 100, 1000\}$, $a, b \in \{0.1, 1, 10\}$ (63 configurations) gives $K^* = 6$ in 46 cases, $K^* = 4$ in 9, $K^* = 8$ in 6 and $K^* = 7$ in 2. All exceptions have small n or $b \ll a$: by Theorem 8.5 the vertex modes have rate $\asymp 3b\sqrt{m}$ and join the slow sector when $3bm \lesssim 2a$, so the six-regime picture requires $m \gg \max(1, a/b)$. The heat trace (Figure 6, left) shows the same: no plateau at $n = 10$, a plateau near 5.6 at $n = 100$ and a sharp plateau at 6 for $n \geq 10^3$, over a range of horizons that widens like m in agreement with (33).

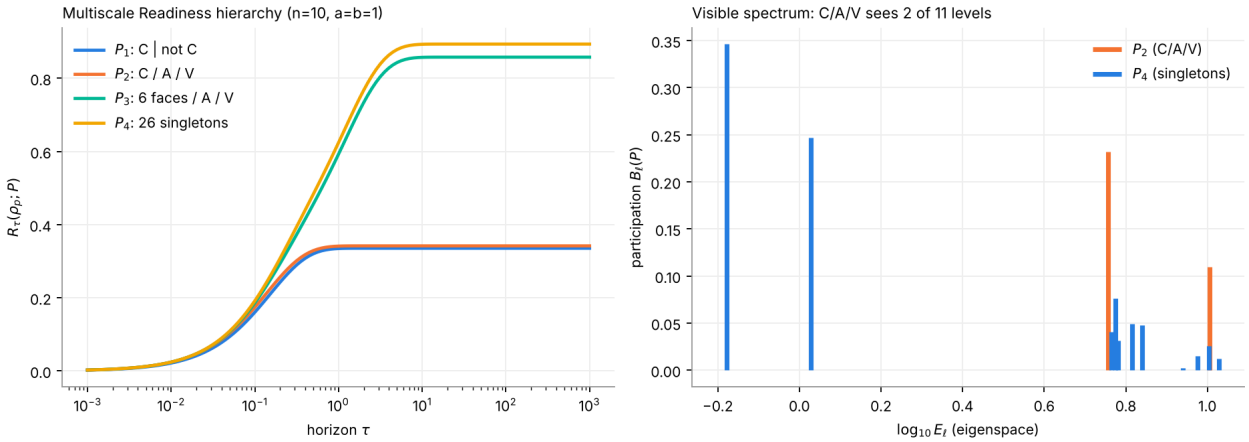

FIGURE 5. Left: multiscale Readiness for $\mathcal{P}_1 \preceq \mathcal{P}_2 \preceq \mathcal{P}_3 \preceq \mathcal{P}_4$. Right: participation $B_\ell(\mathcal{P})$ per eigenspace. The geometric partition sees only the two symmetric fast levels; the singleton partition sees all eleven, and most of its weight sits on the slow octahedral levels ($\log_{10} E \approx -0.19$ and 0.02).

Which regimes. Mapping the six slow eigenfunctions to PCCA memberships with the faces as simplex vertices assigns each face to itself, each edge $\frac{1}{2}$–$\frac{1}{2}$ to its two faces and each vertex $\frac{1}{3}$ to its three faces, exactly as $n \to \infty$ (at $n = 10$: 0.527 and 0.363). The dynamics proposes the six outcomes of the die as regimes, with edges and vertices as transition states. Because E_1 is threefold degenerate, single nodal domains are basis-dependent (any rotation in the T_{1u} eigenspace is admissible), which is why the eigenspace, not the eigenvector, must be used.

Theorem 8.8 (Crisp regimes lose half)**.** *For any crisp partition of the die into six face-basins (each edge and vertex assigned to one adjacent face), $\eta \to \frac{1}{2}$ as $n \to \infty$, while fuzzy PCCA regimes have $\eta = 1$ for every n.*

Proof. Each edge is joined to two faces by links of flux $a\sqrt{p_c p_a} = am^{3/2}/M$; whichever face receives it, the other link is cut and counted in two regimes. Hence $\sum_r \mathrm{cut}(A_r) = 24\, am^{3/2}/M\,(1 + o(1))$, $P_r \to 1/6$ and $J_6 \sim 6 \cdot 24am^{3/2}/(6m^2) = 24a/\sqrt{m}$, whereas $\sum_{\ell=1}^{5} E_\ell \sim 3 \cdot 2a/\sqrt{m} + 2 \cdot 3a/\sqrt{m} = 12a/\sqrt{m}$ by Theorem 8.3. The fuzzy statement is the remark after Theorem 6.2. □

Numerically $\eta_{\mathrm{crisp}} = 0.5236$, 0.5021, 0.50002 at $n = 10, 10^2, 10^4$, and $\eta_{\mathrm{fuzzy}} = 1$ to 10^{-11}. A local search over crisp six-partitions at $n = 10$ found the best $\eta = 0.547$, with $R_\infty = 0.830$, $R'_0 = 1.2056$, $\Lambda_R = 1.453$, $E_R = 0.845$, $\mathcal{H}_R = 0.718$ and minimum regime mass 13.1%; the geometric partition has $\eta = 0.079$, $R_\infty = 0.342$, $\Lambda_R = 7.325$, $E_R = 6.824$, $\mathcal{H}_R = 0.073$. Reorganization between dynamical regimes is about eight times slower than between geometric classes (E_R ratio 8.1), as expected of metastable sets.

8.9. **Synchronization on the die.** Let $\mathcal{P}^x$ and $\mathcal{P}^y$ classify states by $\mathrm{sign}(x)$ and $\mathrm{sign}(y)$. The die is not separable (p is not a product and the graph is not Cartesian), and indeed $\mathcal{S}_\tau(\mathcal{P}^x, \mathcal{P}^y) = 8.1 \times 10^{-4},\ 9.6 \times 10^{-3},\ 4.36 \times 10^{-2}$ at $\tau = 0.05, 0.2, 1$, changing sign at long horizons (-3.4×10^{-3} at $\tau = 5$, -8.9×10^{-3} at $\tau = 20$) as the static term $\mathcal{S}_\infty$ takes over. Bounds (15) hold at every horizon.

9. Inference in practice

9.1. **Estimation.** For a single synthetic trajectory ($n = 10$, $a = 1.3$, $b = 0.6$), the estimators (22) give $\hat{a} = 1.2996$, $\hat{b} = 0.6023$ with 3×10^4 jumps (relative errors 3×10^{-4}, 4×10^{-3}), and $\mathrm{TV}(\hat{p}, p)$ decreasing as $T^{-1/2}$ (0.129, 0.056, 0.014, 0.003 for $T = 10^2, \ldots, 10^5$). Over 300 replicate trajectories

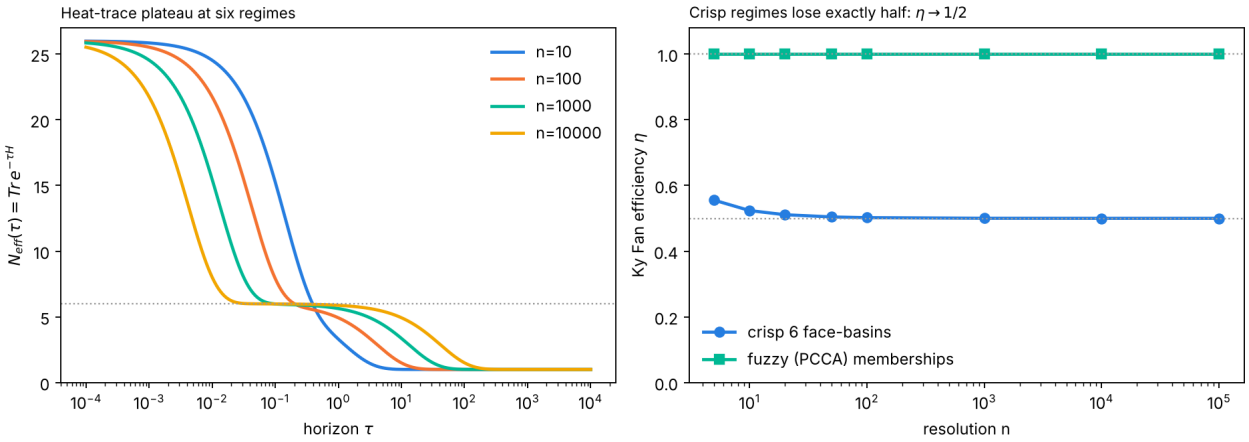

FIGURE 6. Left: heat trace $N_{\mathrm{eff}}(\tau) = \operatorname{Tr} e^{-\tau H}$; a plateau at six develops as n grows. Right: Ky Fan efficiency of crisp face-basin partitions ($\to 1/2$, Theorem 8.8) and of fuzzy PCCA regimes ($= 1$).

of length $T = 300$, the empirical relative variance of $\hat{d}$ on one face–edge pair was 0.0257 against the delta-method prediction (23) of 0.0307; the delta method is conservative at these small counts.

9.2. **Testing.** For the incidence graph of the die, Theorem 7.2 predicts $\Lambda \sim \chi^2_{23}$ under QDS-G. With 60 replicate trajectories ($n = 5$, $T = 3000$) the empirical mean of Λ was 22.68 (theory 23) and the rejection rate at 5% was 1.7%. Under a non-reversible alternative with a 25% circulating bias around the face–edge–vertex cycles, the mean was 582.7 and the power 100% (20 replicates). Finally, 2,000 settling throws of the *absorbing* die ($V \to A \to C$, faces absorbing) produce only one-way transitions on all 48 edges: QDS-G is rejected with certainty, as it must be. The resting die is an irreversible absorption, not a reversible equilibrium; it requires the non-reversible extension discussed below.

9.3. **From the die to markets.** Nothing above depends on the die except the graph and the data. A market observed through volatility, direction and dealer positioning is a Cartesian product graph of $2 \times 3 \times 2$ joint states; Theorem 5.4 gives a null hypothesis for the coupling of its axes, Theorem 7.2 a test for the circulation around its cycles, and the strategic reading of its states is developed, with data, in the companion paper [3].

10. Discussion: what kind of statistics is this?

QDS-G assigns to every observed distribution an operator, to every operator a spectrum, and to every partition of the state space a function of the horizon with a precise probabilistic meaning. The construction differs from classical descriptive statistics in three respects.

It is relational. Readiness is not a property of p alone, but of $(p, \mathcal{G}, D, \mathcal{P})$: the same distribution has different Readiness depending on how states are connected and which distinctions the observer makes. The Krylov theorem quantifies exactly which part of the dynamics a given observer can see.

It is spectral. Every Readiness curve is a positive combination of elementary relaxations $1 - e^{-E\tau}$. Three time scales emerge naturally, and they need not agree: the global gap E_1 (mixing of the whole system), the observable gap E_{obs} (asymptotic decay of reorganization along the chosen boundaries) and the reorganization rate $E_R = 1/T_R$ (the mean time at which reorganization actually occurs). In the die they scale as $m^{-1/2}$, $m^{1/2}$ and $m^{1/2}$ with different constants, and E_{obs} can be carried by a mode of vanishing weight.

It is multiscale and compositional. Partitions form a lattice, and Readiness is monotone on it. Increments between scales are probabilities of reorganizations that exist only at the finer scale; joint regimes obey union and maximum bounds; and the covariance $\mathcal{S}_\tau$ detects coupling between dimensions, vanishing identically for separable systems.

Two structural lessons from the die are general. First, *designed regimes are not dynamical regimes*: the geometric classes are not metastable, the six outcomes are, and the latter are found by the slow eigenspace. Second, *silent refinements are where the slow physics hides*: a refinement that adds no boundary edges leaves the instantaneous Readiness unchanged and reveals only slow reorganization.

The main open direction is non-reversibility. Theorem 7.2 provides the test, the die at rest provides a natural counterexample (Section 9: 2,000 settling throws produce only one-way transitions on all 48 edges), and the cycle affinities $\mathcal{A}_c$, b_1 of them, are the natural extra parameters of a non-reversible QDS: a Hamiltonian with a magnetic (antisymmetric) part on the cycle space of $\mathcal{G}$.

11. Honesty and limitations

All results on the die use a reference lattice distribution and diffusivities chosen by us rather than estimated from physical throws; the rigid-body simulation and estimation from real trajectories are pending. QDS-G is, by Theorem 2.4, a reversible Markov model in Hamiltonian coordinates; its contribution lies in the spectral, geometric and multiscale reading of Readiness and in the inferential apparatus built on it, not in predictive superiority over classical models, which has not been established. Several ingredients are classical in their own fields (ground-state transforms, Kolmogorov's criterion, Wilks' theorem, Cheeger inequalities, Feshbach reductions, PCCA); their assembly into a theory of Readiness, and the results on observable spectra, partition calculus, separability and the die, should still be checked against the literature on reversible chains and metastability [7, 9] before priority is claimed.

Appendix A. QDS-L: a Lindblad extension, first results

A separate experimental line evolves a 26×26 density matrix under $\dot\rho = -i[H_0 + \kappa A, \rho] + \mathcal{D}_{\text{trans}}(\rho) - \gamma(\rho - \operatorname{diag}\rho)$, with H_0 the resting heights $(1, \sqrt{2}, \sqrt{3})$, Lindblad jumps with rates α (towards less stable states) and β (back), on both graphs: $2 \times 2{,}400$ configurations, $\kappa \in \{0, \dots, 2\}$, $\eta, \gamma, \alpha, \beta$ on grids. Trace, Hermiticity and positivity were preserved to 10^{-13}. Populations coincide with the classical chain exactly when $\kappa = 0$ and to $< 10^{-4}$ for $\kappa \le 0.01$. Adiabatic elimination of coherences gives a classical chain with rates $q_{ij} + 2\kappa^2\Gamma_{ij}/(\Gamma_{ij}^2 + \Delta_{ij}^2)$ that absorbs most of the difference (integrated total variation at $\kappa = 2$: $0.108 \to 0.028$); only 15% of the grid departs from it by more than 1%. With zero phases, initial coherence has no effect, since the current $2\,\mathrm{Im}(H_{ij}\rho_{ji})$ vanishes. QDS-L is not part of canonical QDS and should be retained only if it proves superior out of sample.

Appendix B. Computational verification and reproducibility

Ancillary files. The ancillary archive contains the engine `QDS_G.py`, the twelve experiment scripts `G01`–`G12` that produce every check in the table above, the figure scripts, the stand-alone module `qds_graph` and the output files in `results/`. Requirements: Python 3, NumPy, SciPy, pandas, Matplotlib. Each script runs in less than a few minutes on a laptop.

Use of AI tools. The computations, the checks of the proofs and the drafting of this paper were carried out with the assistance of an AI system (Claude, Anthropic), under the author's direction. The author checked the results and takes responsibility for them.

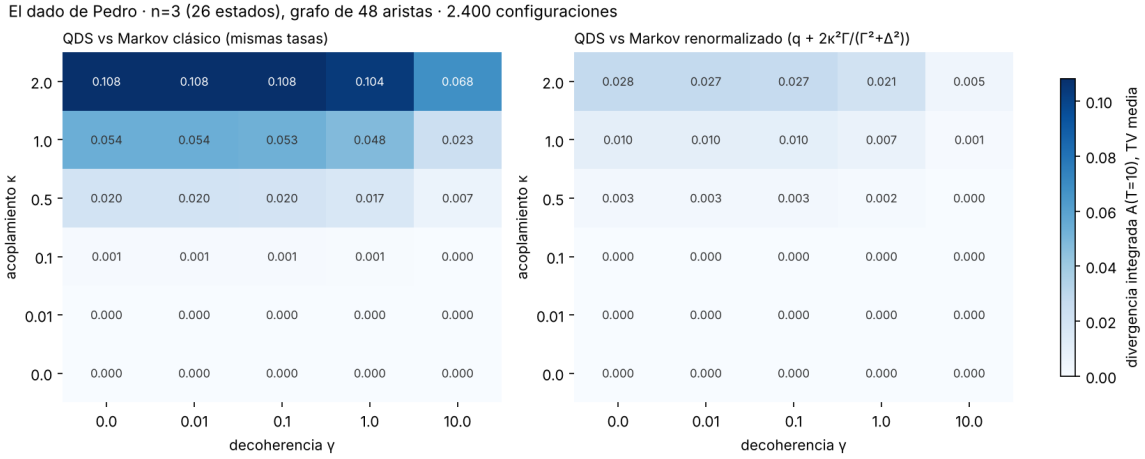

FIGURE 7. QDS-L, $n = 3$, incidence graph: integrated total-variation divergence from the classical chain with the same rates (left) and from the chain with rates renormalised by adiabatic elimination of coherences (right), averaged over η, α, β.

Check	Scope	Max. error
Thms. 2.2–2.4: $H\psi = 0$, $H \succeq 0$, conservation, stationarity, detailed balance, $G_\tau = e^{\tau Q} \geq 0$	400 random (p, D), both graphs	10^{-12}
Exact $26 \to 3$ reduction, (26)	42 parameter sets, $n \leq 10^3$	5×10^{-13}
Spectral Readiness (7) vs. direct propagator	$n \leq 10^3$, $a, b \in [0.01, 10]$	2×10^{-10}
Boundary flux (8), closed forms (34)–(35)	1,408 configurations, $n \leq 10^6$	3×10^{-10}
Bernstein property, spectral sandwich, refinement monotonicity	all of the above	no violation
Krylov dimensions, silent refinement (Table 2)	$n = 10$	exact
Octahedral sector (28), (37); laws (36), (31)	$n \leq 10^6$, 5 (a, b) pairs	$O(m^{-1})$
Separability (17), $\mathcal{S}_\tau \equiv 0$	12-state market graph	5×10^{-16}
Reversibility LRT, χ^2_{23}	60 null + 20 alternative runs	see text
Irrep block spectrum (Theorem 8.5)	200 random (n, a, b)	2×10^{-15}
Γ_6 law (33); $\mathcal{H}_R$ identity; Ky Fan; $\eta \to \frac{1}{2}$	$m \leq 10^5$, 4 (a, b)	$O(m^{-1})$; 10^{-15}
K^* distribution	63 configurations	exact

REFERENCES

[1] P. Caceres, *Quantum Data Statistics*, HAL preprint hal-05457132 (13 January 2026); revised as *Quantum Data Statistics, Part 0: Foundations*, v12, manuscript (November 2026).

[2] P. Caceres, *QDS Formula Sheet*, v4, manuscript (November 2026).

[3] P. Caceres, *QDS Stocks: a quantum approach to investments*, companion preprint (November 2026).

[4] R. L. Schilling, R. Song, Z. Vondraček, *Bernstein Functions: Theory and Applications*, 2nd ed., de Gruyter (2012).

[5] G. F. Lawler, A. D. Sokal, Bounds on the L^2 spectrum for Markov chains and Markov processes: a generalization of Cheeger's inequality, *Trans. Amer. Math. Soc.* 309 (1988) 557–580.

[6] P. Deuflhard, M. Weber, Robust Perron cluster analysis in conformation dynamics, *Linear Algebra Appl.* 398 (2005) 161–184.

[7] D. A. Levin, Y. Peres, E. L. Wilmer, *Markov Chains and Mixing Times*, 2nd ed., AMS (2017).

[8] R. R. Coifman, S. Lafon, Diffusion maps, *Appl. Comput. Harmon. Anal.* 21 (2006) 5–30.

[9] A. Bovier, F. den Hollander, *Metastability: A Potential-Theoretic Approach*, Springer (2015).
[10] A. Kolmogorov, Zur Theorie der Markoffschen Ketten, *Math. Ann.* 112 (1936) 155–160.
[11] S. S. Wilks, The large-sample distribution of the likelihood ratio for testing composite hypotheses, *Ann. Math. Statist.* 9 (1938) 60–62.

Universidad Europea de Valencia, Valencia, Spain
Email address: pedrojesus.caceres@universidadeuropea.es
URL: https://orcid.org/0000-0002-6540-8993